Electronic band structure of Two-Dimensional WS_2/Graphene van der Waals Heterostructures

Hugo Henck,[1] Zeineb Ben Aziza,[1] Debora Pierucci,[2] Feriel Laourine,[1] Francesco Reale,[3] Pawel Palczynski,[3] Julien Chaste,[1] Mathieu G. Silly,[4] François Bertran,[4] Patrick Le Fèvre,[4] Emmanuel Lhuillier,[5] Taro Wakamura,[6] Cecilia Mattevi,[3] Julien E. Rault,[4] Matteo Calandra,[5] and Abdelkarim Ouerghi[1,*]

[1]*Centre de Nanosciences et de Nanotechnologies, CNRS, Université Paris-Sud, Université Paris-Saclay, C2N–Marcoussis, 91460 Marcoussis, France*

[2]*CELLS–ALBA Synchrotron Radiation Facility, Carrer de la Llum 2-26, 08290 Cerdanyola del Valles, Barcelona, Spain*

[3]*Imperial College London, Department of Materials, Exhibition Road, London SW7 2AZ, United Kingdom*

[4]*Synchrotron-SOLEIL, Saint-Aubin, Boîte Postale 48, F91192 Gif sur Yvette Cedex, France*

[5]*Sorbonne Universités, UPMC Université Paris 06, CNRS-UMR 7588, Institut des NanoSciences de Paris, 4 Place Jussieu, 75005 Paris, France*

[6]*Laboratoire de Physique des Solides, CNRS, Université Paris-Sud, Université Paris Saclay, 91405 Orsay Cedex, France*

(Received 26 October 2017; revised manuscript received 8 February 2018; published 19 April 2018)

Combining single-layer two-dimensional semiconducting transition-metal dichalcogenides (TMDs) with a graphene layer in van der Waals heterostructures offers an intriguing means of controlling the electronic properties through these heterostructures. Here, we report the electronic and structural properties of transferred single-layer WS_2 on epitaxial graphene using micro-Raman spectroscopy, angle-resolved photoemission spectroscopy measurements, and density functional theory (DFT) calculations. The results show good electronic properties as well as a well-defined band arising from the strong splitting of the single-layer WS_2 valence band at the K points, with a maximum splitting of 0.44 eV. By comparing our DFT results with local and hybrid functionals, we find the top valence band of the experimental heterostructure is close to the calculations for suspended single-layer WS_2. Our results provide an important reference for future studies of electronic properties of WS_2 and its applications in valleytronic devices.

DOI: 10.1103/PhysRevB.97.155421

I. INTRODUCTION

Two-dimensional (2D) materials, such as graphene, h-BN, phosphorene, and transition-metal dichalcogenides (TMDs), are an ideal platform for studying exciting physical properties not attainable in their bulk counterparts [1]. They often exhibit a versatile electronic structure controllable by thickness [2], surface chemical adsorption, and strain [3]. Of particular interest is the family of TMDs of formula $MX_2 (M = \mathrm{Mo,W}; X = \mathrm{S,Se})$. They are semiconductors with unique properties in the 2D limit such as indirect to direct band-gap transition, large exciton binding energy, well-defined valley degrees of freedom, and spin splitting of the valence band [4]. Many efforts have been made to harvest these properties into practical optoelectronic, spintronic, and valleytronic devices [5].

Thanks to the weak interlayer coupling, these materials can be vertically stacked to form van der Waals (vdW) heterostructure circumventing the limitation induced by large lattice mismatch [1,6]. This gives rise to a completely new paradigm in which the individual properties of each 2D layer are combined to create new device. In particular, the efficient charge transfer capability of monolayer graphene [7] can be combined with a direct band gap of single layer WS_2 in a WS_2/graphene vertical heterostructure to yield efficient photodetectors, where electrons and holes are readily created and separated [8,9].

MX_2 single layer, the elementary unit that forms ultrathin films by weak stacking, features a novel spin-valley coupled band structure. At the corners of the first Brillouin zone (BZ), the valence (conduction) band has two inequivalent valleys. Owing to the broken inversion symmetry in single layers, the strong spin-orbit coupling (SOC) from the d orbitals of the metal atoms results in a valence-band spin splitting at the K points, with a magnitude as large as 400 meV in WS_2 [10,11]. The spin splitting has opposite signs at the K and K' valleys as they are a time reversal of each other at the valence band. This spin-valley coupling forms the basis for manipulation of spin and valley degrees of freedom in these 2D semiconductors.

Angle-resolved photoemission spectroscopy (ARPES) is one of the most suitable tools to investigate the electronic structure of 2D materials with energy and momentum resolution as well as surface sensitivity [12–15]. There have been a number of ARPES studies either on bulk MX_2 samples or few-layer samples prepared by various methods such as exfoliation, chemical vapor deposition (CVD) [16,17], and epitaxial growth [18,19]. They all observe sizable splitting in the valence band (VB) at the K point, with a size of $\sim$150 meV for MoS_2 and $\sim$400 meV for WS_2 as tungsten induces larger SOC [20]. Furthermore, uniform and large-area synthesis of single-layer WS_2 is an important subject in applications of 2D materials in various electronic devices [21].

*abdelkarim.ouerghi@c2n.upsaclay.fr

II. METHODS

Single-layer graphene was produced via a two-step process beginning with a starting substrate of 4H-SiC(0001). Prior to graphitization, the substrate was hydrogen etched (100% H_2) at 1550 °C to produce well-ordered atomic terraces of SiC. Subsequently, the SiC sample was heated to 1000 °C and then further heated to 1550 °C in an Ar atmosphere [22–24]. WS_2/SiO_2 samples were grown by chemical vapor deposition (CVD) in a 1-in. quartz tube furnace. The growth substrate was placed in the center of the furnace and heated to 800 °C. A 25-mg sulfur pellet was placed on a piece of silicon and positioned upstream in the furnace such that its temperature was approximately 150 °C. Carrier gas (500 sccm N_2) was used to bring sulfur vapor into the furnace for a 30-min growth period [25].

The ARPES measurements were conducted at the CASSIOPEE beamline of Synchrotron SOLEIL (Saint-Aubin, France). We used linearly polarized photons of 50 eV and a hemispherical electron analyzer with vertical slits to allow band mapping. The total angle and energy resolutions were 0.25° and 10 meV. All ARPES experiments were done at low temperature (8 K). X-ray photoelectron spectroscopy (XPS) experiments were carried out on the TEMPO beamline of Synchrotron SOLEIL (Saint-Aubin, France) at room temperature. The photon source was a HU80 Apple II undulator set to deliver linearly polarized light. The photon energy was selected using a high-resolution plane grating monochromator with a resolving power $E/\Delta E$ that can reach 15000 on the whole energy range (45–1500 eV). During the XPS measurements, the photoelectrons were detected at 0° from the sample surface normal $\vec{n}$ and at 46° from the polarization vector $\vec{E}$.

III. RESULTS AND DISCUSSIONS

In this work, TMD/graphene heterostructures were made from WS_2 grown by CVD on SiO_2/Si substrates that were then transferred onto graphene/SiC [26] (more details about the transfer procedure are given in the Supplemental Material, Sec. I [27]). A schematic of WS_2 crystal structure is presented in Fig. 1(a) where the lattice constants are indicated. The CVD growth of WS_2 on SiO_2 results in characteristic single-crystal domains shaped as well-defined equilateral triangles [28]. These films can be nondestructively transferred to various kinds of substrates as desired. With respect to SiO_2 and similar substrates, the graphene layer has favorable qualities such as atomic flatness, and homogeneous charge distribution. This should enable direct investigation of the adjacent TMD's intrinsic electronic structure and many-body effects. The graphene layer is often used as a substrate for TMD heterostructures with high device performance [29]. Single-layered WS_2 flakes were then easily identified by their optical contrast with respect to the graphene substrate [Fig. 1(b)] and confirmed by micro-Raman spectroscopy [Figs. 1(c) and 1(d)]. The optical image in Fig. 1(b) shows large (lateral size about 50 μm) triangular flakes of WS_2 on the graphene layer. The graphene underlayer used in this study was obtained by annealing 4H-SiC(0001) (see the Methods section). After the transfer of WS_2 onto graphene, an annealing process at $T = 300\,^{\circ}C$ for 60 min in UHV was used to further clean the surface and interface of the WS_2/graphene heterostructure. To investigate the structural properties of the WS_2 flakes micro-Raman and photoluminescence (PL) spectroscopy [30–33] were used (Figs. 1(c) and 1(d) and Supplemental Material, Secs. II and III [27]). Several Raman spectra of WS_2 on graphene, collected in different flake positions, are shown in Fig. 1(c). These Raman spectra are obtained with 532-nm excitation, which is in resonance with the B exciton absorption peak [34,35]. Then, beside the first-order modes at the Brillouin zone (BZ) center (Γ), the in-plane phonon mode E^1_{2g} at 356 cm^{-1}, and the out-of-plane phonon mode A_{1g} at 418 cm^{-1} [36,37], the Raman spectra present a series of overtone and combination peaks. These different contributions are clearly separated using a multipeak Lorentzian fit [blue lines in Fig. 1(c), top]. In particular, the Raman feature around 350 cm^{-1} is the convolution of several components: the E^1_{2g} (Γ), the 2 LA (M) mode at 351.7 cm^{-1}, which is a second-order Raman mode due to LA phonons at the M point of the BZ zone, and the E^1_{2g} (M) mode [38]. Moreover, Raman peaks at 323.7 and 297.1 cm^{-1} are combinations modes, which are attributed to 2LA (M) $- E^2_{2g}$ (Γ) and the 2LA (M) $- 2E^2_{2g}$ (Γ) modes, respectively. Raman mapping was conducted to investigate the uniformity within the single flake [39–42]. The 2LA (M), E^1_{2g} (Γ), and the A_{1g}(Γ) modes' intensity and position mapping are shown in Figs. 1(d) and S2 [27]. These Raman modes' peak positions and intensity are uniform within the single crystal, indicating that the electronic properties of WS_2 are uniform on the graphene substrate. From the frequency difference between A_{1g}(Γ) and 2LA (M), the thickness of the WS_2 flakes can be determined [43–45]. An average distance of 65.9 ± 0.1 cm^{-1} is obtained, as shown in Fig. S4 [27]. This value is consistent with monolayer WS_2 as already shown by previous studies [46]. For the following experiments, the single-layer coverage was estimated to be around 20% of the total area of the sample.

The high quality of the WS_2 transferred on a graphene layer allows investigating the electronic structure by x-ray photoelectron spectroscopy (XPS) and ARPES. Both the feasible large-area synthesis and the reliable film transfer process can promise that WS_2 ultrathin films will pave a route to many applications of 2D materials and vdW heterostructure. XPS is used to determine the chemical composition and stoichiometry of the WS_2 films transferred on the graphene. The C-1s XPS spectrum of WS_2 /graphene heterostructure, collected at $h\nu =$ 340 eV, is shown in Fig. 2(a). The C-1s spectrum showed three components at 283.9, 284.7, and 285.1 eV in binding energy (BE). These components correspond to the SiC bulk (labeled SiC), the graphene layer (labeled G), and the interface layer (labeled I), respectively. The G peak was fitted by a sum of a Gaussian function convoluted with a Doniach-Sunjic line shape with an asymmetry factor α of 0.09 and a full width at half maximum (FWHM) of 0.4 eV. The low value of the FWHM indicates that only one core level peak was present and thus the carbon atoms had a unique chemical environment. Moreover, no structure appeared at ∼286.7 eV in the C-1s XPS spectrum, usually attributed to the contamination and/or oxidation; this means even if the samples were annealed at 300 °C, the WS_2/graphene layers were very inert and did not show any contamination after the WS_2 transfer process.

The W-4f and S-2p XPS peaks deconvolution shown in Figs. 2(b) and 2(c), presents the standard WS_2 stoichiometry.

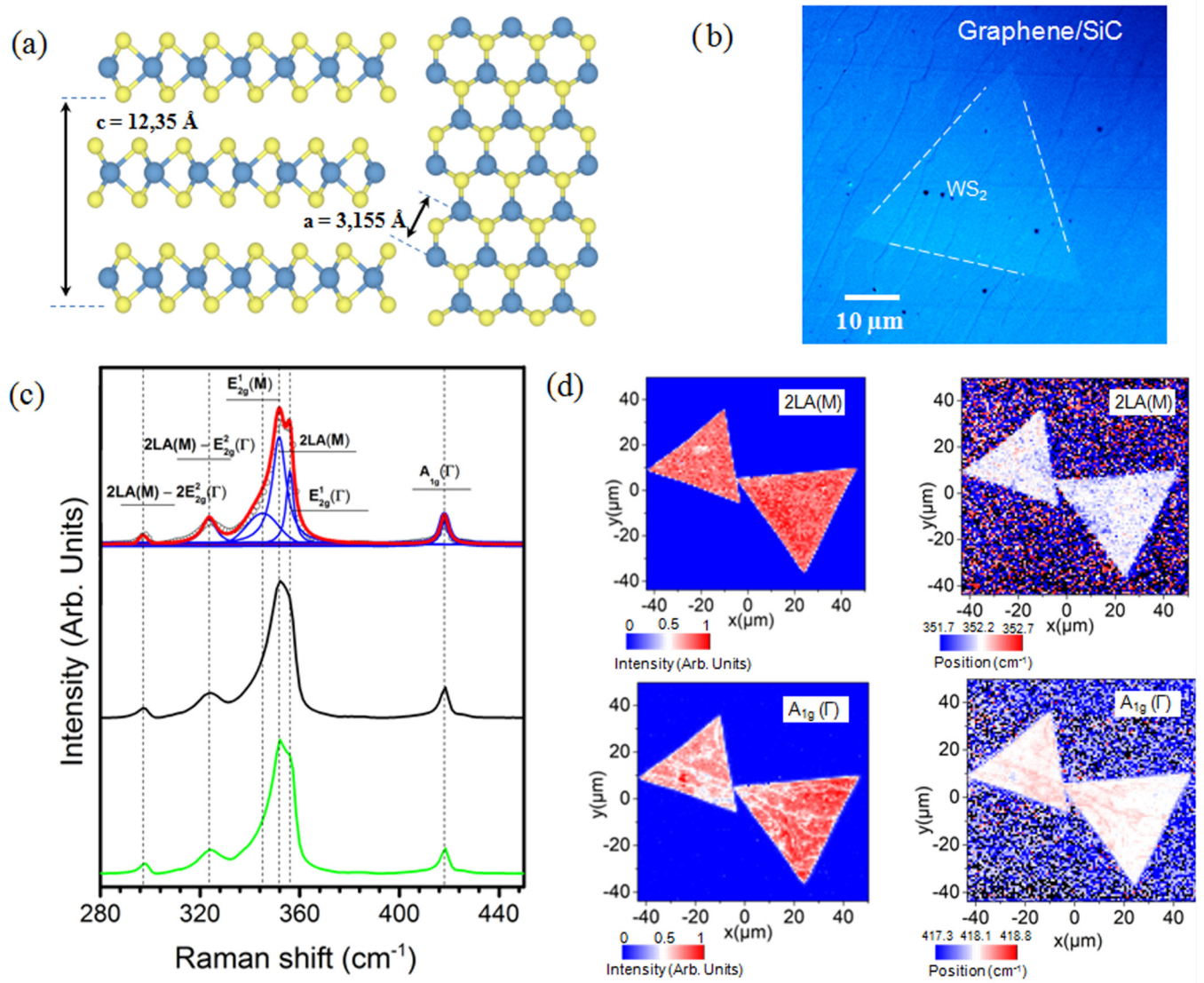

FIG. 1. Structural and electronic properties of a WS_2/graphene heterostructure: (a) crystalline structure of WS_2; (b) typical optical image of the WS_2 transferred onto the graphene layer. The contrast has been adjusted in order to improve the visibility of the flake. The WS_2 profile is traced by white dashed lines. (c) Micro-Raman spectra taken at different positions of the WS_2/graphene heterostructure; in the top spectrum the used multipeak Lorentzian fit is shown as blue lines. (d) Raman map images of the peak intensity and position of the 2LA (M) (top) and $A_{1g}(\Gamma)$ (bottom) modes of WS_2 on epitaxial graphene.

The WS_2 is well fitted by doublet peaks at a BE of 33.4 and 35.6 eV, corresponding to W-4$f_{7/2}$,W-4$f_{5/2}$ core energy levels ($4f_{5/2} : 4f_{7/2}$ ratio of 0.75) [47], respectively [Fig. 2(b)]. The sulfur S-2p peak [Fig. 2(c)] consists of a single doublet (S$-2p_{3/2}$ at a BE $=$ 163 eV and a $2p_{1/2} : 2p_{3/2}$ ratio of 0.5 and spin-orbit splitting of 1.19 eV) corresponding to S-W bonding, and confirms the presence of WS_2. The absence of the oxygen content [48,49] in these samples is a result of the high quality of the interface in this hybrid heterostructure, particularly in light of the Raman characteristics that are comparable to high-quality WS_2 (see above and Supplemental Material, Sec. II [27], and Ref. [50]).

The electronic structure was also probed using ARPES measurements. The WS_2 flakes are relatively well spaced on the graphene substrate, ensuring, thanks to the small spot size ($50 \times 50\,\mu m^2$), the mapping of a single flake. Figure 2(d) shows the photoelectron intensity as a function of energy and k momentum around the normal emission. This is a good measure of the band structure of WS_2 around Γ. The zero of binding energy (i.e., the Fermi level) was determined by fitting the leading edge of the graphene layer at the same photon energies and under the same experimental conditions. Beside the typical dispersion of the π bands of graphene around -6 to -8 eV (most intense band), a new set of bands is visible at the Γ point of the BZ, which is the signature of the WS_2 valence band. In the spectra, the most distinct features include the valence-band maximum (VBM) at Γ. The full width at half maximum (FWHM) of the WS_2 band branches is about 80 meV as shown by the energy distribution curves (EDCs) in Fig. S7 [27]) extracted from the ARPES map of Fig. 2(d) at the Γ point. The sharpness of the different bands can be attributed to the high quality of the transferred flake. Figure 2(e) shows

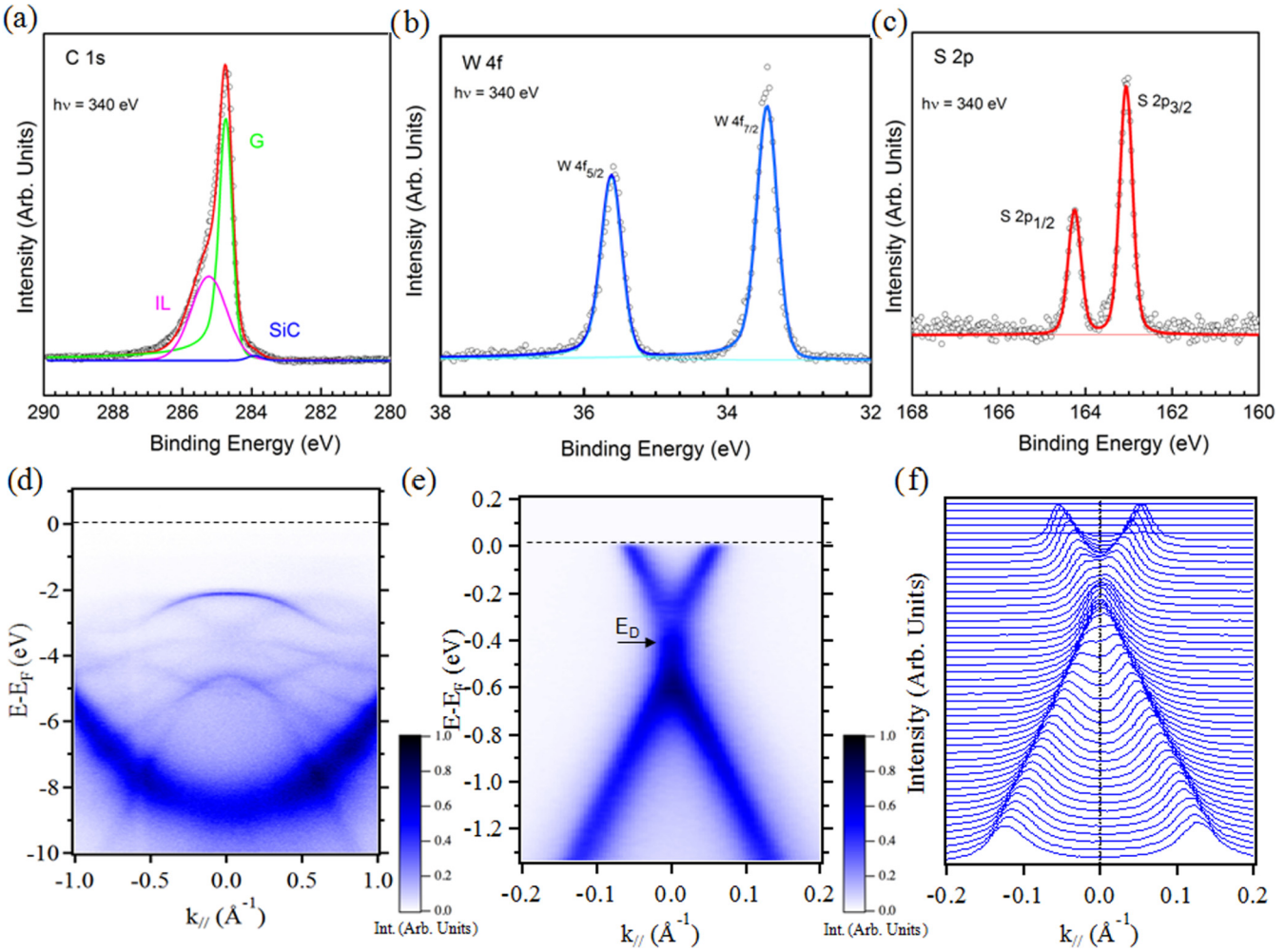

FIG. 2. High-resolution XPS and ARPES of WS_2/graphene heterostructures: (a) C−1*s*, (b) W-4*f*, and (c) S-2*p* core levels at $h\nu = 340$ eV. (d) ARPES map of WS_2/graphene heterostructure around the Γ point in the Γ*K* high-symmetry direction of the WS_2 Brillouin zone. (e) Band structure of the graphene layer in the heterostructure at the Γ*K* high-symmetry direction. (f) Corresponding momentum distribution curves (MDCs) of (e).

the measured band structure corresponding to the graphene underlayer. The single and robust Dirac cone confirms that the graphene monolayer at the heterostructure preserves the Dirac linear dispersion and the massless relativistic character of the graphene carriers close to the Fermi level. The Dirac point (E_D) is located at 0.40 eV below the Fermi level as in the case of pristine graphene on SiC [12]. Then, the *n*-type doping (close to $9 \times 10^{12}\,\mathrm{cm}^{-2}$) of pristine graphene was not modified by the formation of the heterostructure. This confirms, as shown also by the work function measurement (see Supplemental Material, Fig. S8 [27]), that there was no significant charge transfer between the 2D materials. However, if we look more in detail at the momentum distribution curves (MDCs) shown in Fig. 2(f) a less dispersive behavior of the peaks is present around E_D. Then, the presence of a gaplike feature at the *K* point (already present in the pristine graphene) cannot be completely excluded [51]. However, a more detailed study of this feature goes beyond the scope of this paper. From a linear fitting of the MDCs a Fermi velocity $v_F \sim 1.05 \times 10^6$ m/s was also determined.

It is obvious that also the sharp and intense structure of π bands confirms the high structural quality of the WS_2/graphene heterostructure. Differently from our previous work on the MoS_2/graphene layer and from Diaz *et al.* [12,52] no signature of interlayer hybridization and minigaps opening [53] is present on the π band of graphene. The absence of these superperiodicity effects probably is related to the mismatch angle between the WS_2 flake and the graphene underlayer. In the following discussions regarding the ARPES data, we will focus mostly on the split of the valence-band feature at the *K* point of the WS_2 (Fig. 3). In particular, in order to gain more insight on the electronic structure of WS_2, we performed first principles electronic structure calculations on an isolated WS_2 monolayer using the QUANTUM ESPRESSO code [54,55] and Perdew, Burke, and Ernzerhof (PBE) [56] and HSE06 [57] hybrid functionals within the adaptive compressed exchange [58] implementation. More technical details are given in the Supplemental Material (Sec. IV [27]) [59–61]. Figure 3(a) shows the measured band structure around the *K* valley. The top of the valence band at the *K* point is mostly formed by

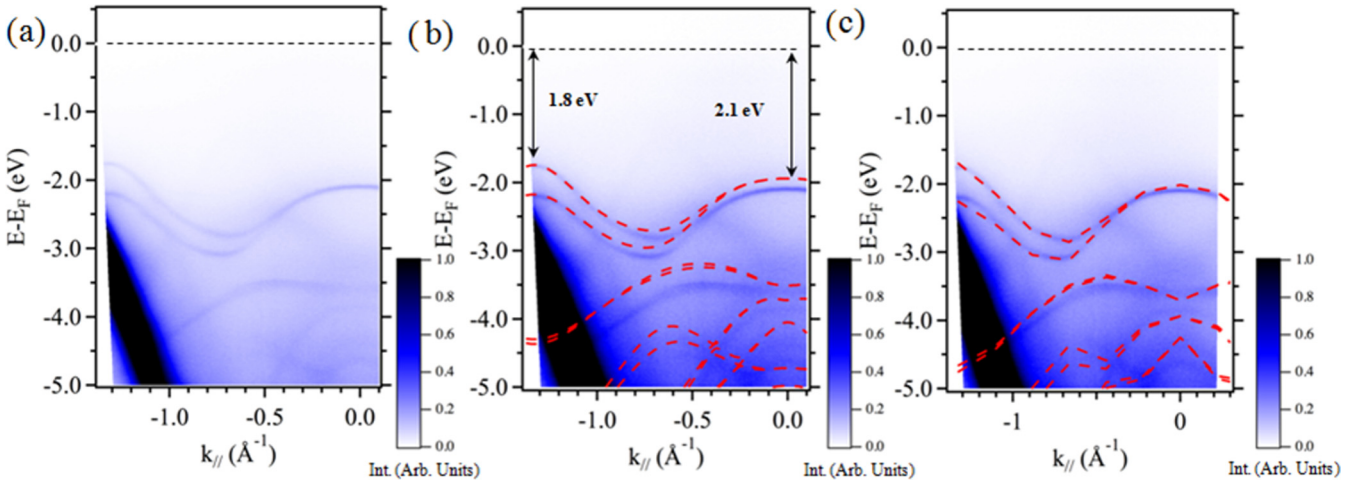

FIG. 3. (a) ARPES map of single-layer WS_2 along the ΓK high-symmetry directions. (b,c) Comparison between ARPES map and DFT calculations (PBE and HSE06, respectively).

the planar d_{xy} and d_{x2-y2} orbitals of tungsten, while at the Γ point the band is mostly composed of W d_z orbitals and S p_z orbitals.

The observation of a single valence band at Γ with a higher binding energy than at K also excludes the contribution from bilayer or trilayer WS_2. In bilayer TMD systems, the valence band near Γ shows a bonding-antibonding splitting that would be observable by ARPES as two bands, in contrast to what is seen here [15]. The maximum of the valence band is located at the K point (–1.8 eV, which is 0.3 eV higher than at the Γ point). Referring to previous works concerning the band gap of single WS_2 [62,63], these measurements indicate that our sample is heavily electron doped, which is consistent with previous reports [64]. The electronic structure in the -2 to -3 eV binding energy range is globally in good agreement with our electronic structure calculations [Figs. 3(b) and 3(c)], although the energy separation between the top of the valence band at K and Γ is slightly underestimated in PBE [Fig. 3(b)]. In both theory and experiments the valence-band maximum at the Γ point is located at higher binding energies than that at the K point, the energy separation between the two being 0.20 eV in experiments [Figs. 3(b) and 3(c)], 0.17 eV in PBE, and 0.20 eV in HSE [Fig. 3(c)]. The measured spin-orbit splitting at K is about 440 meV. Our theoretical calculations for the isolated WS_2 monolayer lead to splittings of 440 meV (PBE) and 551 meV (HSE06 on top of PBE).

Moreover, an analysis of the curvature of the bands from the ARPES measurements also allows us to deduce the effective mass of the single-layer WS_2 forming the heterostructure. We determined an experimentally derived hole effective mass of $0.4\,m_0$ (upper band) and $0.5\,m_0$ (lower band) (where m_0 is the free electron mass) at K, and a hole effective mass of $1.7\,m_0$ at Γ. These values agree very well with the PBE calculated bands, suggesting that many-body effects are not important close to the top of the valence band at K. Finally, the gap between the two highest-energy valence bands and the bands at lower energies is substantially underestimated in PBE. The inclusion of the exchange interaction within the HSE06 functional on top of the PBE geometry corrects both errors but leads to a somewhat too large spin-orbit coupling. Although we cannot include explicitly the interaction with the substrate as we miss the structural orientation between WS_2 and graphene, it seems that the measured ARPES data agree well with the bands of an isolated single layer with PBE geometry and electronic structure obtained with the inclusion of the exchange interaction. In particular the exchange interaction seems to improve the agreement not only for the top of the valence band at the zone center but also for the electronic structure in the binding energy region below -3 eV.

IV. CONCLUSIONS

In summary, we have studied the electronic structure of single-layer WS_2 on epitaxial graphene. We found that this heterostructure gives rise to sharp bands, in particular for the WS_2 VBM near the Γ and K points. We directly observe the strong spin splitting of the upper VB and its values are in excellent agreement with the PBE DFT calculations. Our ARPES measurements on the heterostructure showed graphene and WS_2 largely retained their original electronic structure and, in particular, the suspended WS_2 monolayer is a good approximation of the electronic properties close to the top of the valence band. Finally, we experimentally determined spin-orbit splitting. Our results provide an important reference for future studies of electronic properties of WS_2 and their applications in spintronic and valleytronic devices.

ACKNOWLEDGMENTS

We acknowledge support from the Agence Nationale de la Recherche (ANR) under grants from Labex Nanosaclay and H2DH (Grant No. ANR-15-CE24-0016), from the Region Ile-de-France in the framework of C'Nano IdF (nanoscience competence center of Paris Region). Labex Nanoscalay belongs to the publicly funded Investissements d'Avenir program managed by ANR. C.M. would like to acknowledge the EPSRC award, EP/M022250/1, the EPSRC-Royal Society Fellowship Engagement Grant EP/L003481/1 and the award of a Royal Society University Research Fellowship by the UK Royal Society.

[1] A. K. Geim and I. V. Grigorieva, Van der Waals heterostructures, Nature **499**, 419 (2013).

[2] H. Li, Q. Zhang, C. C. R. Yap, B. K. Tay, T. H. T. Edwin, A. Olivier, and D. Baillargeat, From bulk to monolayer MoS_2: Evolution of Raman scattering, Adv. Funct. Mater. **22**, 1385 (2012).

[3] E. V Castro, K. S. Novoselov, S. V Morozov, N. M. R. Peres, J. M. B. L. Santos, J. Nilsson, A. K. Geim, and A. H. C. Neto, Biased Bilayer Graphene: Semiconductor with a Gap Tunable by the Electric Field Effect, Phys. Rev. Lett. **99**, 216802 (2007).

[4] L. Yang, N. A. Sinitsyn, W. Chen, J. Yuan, J. Zhang, J. Lou, and S. A. Crooker, Long-lived nanosecond spin relaxation and spin coherence of electrons in monolayer MoS_2 and WS_2, Nat. Phys. **11**, 830 (2015).

[5] J. He, D. He, Y. Wang, and H. Zhao, Probing effect of electric field on photocarrier transfer in graphene-WS_2 van der Waals heterostructures, Opt. Express **25**, 1949 (2017).

[6] G. Froehlicher, E. Lorchat, and S. Berciaud, Charge Versus Energy Transfer in Atomically Thin Graphene-Transition Metal Dichalcogenide van der Waals Heterostructures, Phys. Rev. X **8**, 011007 (2018).

[7] E. Pallecchi, F. Lafont, V. Cavaliere, F. Schopfer, D. Mailly, W. Poirier, and A. Ouerghi, High electron mobility in epitaxial graphene on 4H-SiC(0001) via post-growth annealing under hydrogen, Sci. Rep. **4**, 4558 (2014).

[8] T. Georgiou, R. Jalil, B. D. Belle, L. Britnell, R. V Gorbachev, S. V Morozov, Y.-J. Kim, A. Gholinia, S. J. Haigh, O. Makarovsky *et al.*, Vertical field-effect transistor based on graphene-WS_2 heterostructures for flexible and transparent electronics, Nat. Nanotechnol. **8**, 100 (2012).

[9] Z. Hu, Q. Liu, S.-L. Chou, and S.-X. Dou, Advances and challenges in metal sulfides/selenides for next-generation rechargeable sodium-ion batteries, Adv. Mater. **29**, 1700606 (2017).

[10] S. Ulstrup, J. Katoch, R. J. Koch, D. Schwarz, S. Singh, K. M. McCreary, H. K. Yoo, J. Xu, B. T. Jonker, R. K. Kawakami *et al.*, Spatially resolved electronic properties of single-layerWS_2on transition metal oxides, ACS Nano **10**, 10058 (2016).

[11] J. Katoch, S. Ulstrup, R. J. Koch, S. Moser, K. M. McCreary, S. Singh, J. Xu, B. T. Jonker, R. K. Kawakami, A. Bostwick *et al.*, Giant spin-splitting and gap renormalization driven by trions in single-layer WS_2/h-BN heterostructures, Nat. Phys. **14**, 355 (2018).

[12] D. Pierucci, H. Henck, J. Avila, A. Balan, C. H. Naylor, G. Patriarche, Y. J. Dappe, M. G. Silly, F. Sirotti, A. T. C. Johnson *et al.*, Band alignment and minigaps in monolayer MoS2-graphene van der Waals heterostructures, Nano Lett. **16**, 4054 (2016).

[13] A. Grubišić Čabo, J. A. Miwa, S. S. Grønborg, J. M. Riley, J. C. Johannsen, C. Cacho, O. Alexander, R. T. Chapman, E. Springate, M. Grioni *et al.*, Observation of ultrafast free carrier dynamics in single layer MoS_2, Nano Lett. **15**, 5883 (2015).

[14] W. Jin, P.-C. Yeh, N. Zaki, D. Chenet, G. Arefe, Y. Hao, A. Sala, T. O. Mentes, J. I. Dadap, A. Locatelli *et al.*, Tuning the electronic structure of monolayer graphene/MoS_2 van der Waals heterostructures via interlayer twist, Phys. Rev. B **92**, 201409 (2015).

[15] P. C. Yeh, W. Jin, N. Zaki, D. Zhang, J. T. Liou, J. T. Sadowski, A. Al-Mahboob, J. I. Dadap, I. P. Herman, P. Sutter *et al.*, Layer-dependent electronic structure of an atomically heavy two-dimensional dichalcogenide, Phys. Rev. B **91**, 041407(R) (2015).

[16] S. Forti, A. Rossi, H. Büch, T. Cavallucci, F. Bisio, A. Sala, T. O. Menteş, A. Locatelli, M. Magnozzi, M. Canepa *et al.*, Electronic properties of single-layer tungsten disulfide on epitaxial graphene on silicon carbide, Nanoscale **9**, 16412 (2017).

[17] A. Rossi, D. Spirito, F. Bianco, S. Forti, F. Fabbri, H. Büch, A. Tredicucci, R. Krahne, and C. Coletti, Patterned tungsten disulfide/graphene heterostructures for efficient multifunctional optoelectronic devices, Nanoscale **10**, 4332 (2018).

[18] K. Liu, Q. Yan, M. Chen, W. Fan, Y. Sun, J. Suh, D. Fu, S. Lee, J. Zhou, S. Tongay *et al.*, Elastic properties of chemical-vapor-deposited monolayer MoS_2,WS_2, and their bilayer heterostructures, Nano Lett. **14**, 5097 (2014).

[19] M. T. Dau, C. Vergnaud, A. Marty, F. Rortais, C. Beigné, H. Boukari, E. Bellet-Amalric, V. Guigoz, O. Renault, C. Alvarez *et al.*, Millimeter-scale layered $MoSe_2$ grown on sapphire and evidence for negative magnetoresistance, Appl. Phys. Lett. **110**, 11909 (2017).

[20] K. Chen, X. Wan, J. Wen, W. Xie, Z. Kang, X. Zeng, H. Chen, and J.-B. Xu, Electronic properties of $MoS_2 - WS_2$ heterostructures synthesized with two-step lateral epitaxial strategy, ACS Nano **9**, 9868 (2015).

[21] X. Zhang, F. Meng, J. R. Christianson, C. Arroyo-Torres, M. A. Lukowski, D. Liang, J. R. Schmidt, and S. Jin, Vertical heterostructures of layered metal chalcogenides by van der Waals epitaxy, Nano Lett. **14**, 3047 (2014).

[22] H. Sediri, D. Pierucci, M. Hajlaoui, H. Henck, G. Patriarche, Y. J. Dappe, S. Yuan, B. Toury, R. Belkhou, M. G. Silly *et al.*, Atomically sharp interface in an h-BN-epitaxial graphene van der Waals heterostructure, Sci. Rep. **5**, 16465 (2015).

[23] E. Pallecchi, M. Ridene, D. Kazazis, C. Mathieu, F. Schopfer, W. Poirier, D. Mailly, and A. Ouerghi, Observation of the quantum Hall effect in epitaxial graphene on SiC(0001) with oxygen adsorption, Appl. Phys. Lett. **100**, 253109 (2012).

[24] D. Pierucci, H. Sediri, M. Hajlaoui, E. Velez-Fort, Y. J. Dappe, M. G. Silly, R. Belkhou, A. Shukla, F. Sirotti, N. Gogneau *et al.*, Self-organized metal–semiconductor epitaxial graphene layer on off-axis 4H-SiC (0001), Nano Res. **8**, 1026 (2015).

[25] F. Reale, P. Palczynski, I. Amit, G. F. Jones, J. D. Mehew, A. Bacon, N. Ni, P. C. Sherrell, S. Agnoli, M. F. Craciun, S. Russo, and C. Mattevi, High-mobility and high-optical quality atomically thin WS_2, Sci. Rep. **7**, 14911 (2017).

[26] D. Pierucci, H. Henck, C. H. Naylor, H. Sediri, E. Lhuillier, A. Balan, J. E. Rault, Y. J. Dappe, F. Bertran, P. Le Fèvre *et al.*, Large area molybdenum disulphide-epitaxial graphene vertical Van der Waals heterostructures, Sci. Rep. **6**, 26656 (2016).

[27] See Supplemental Material at http://link.aps.org/supplemental/10.1103/PhysRevB.97.155421 for details on the fabrication process, measurements, and calculations.

[28] G. H. Han, N. J. Kybert, C. H. Naylor, B. S. Lee, J. Ping, J. H. Park, J. Kang, S. Y. Lee, Y. H. Lee, R. Agarwal *et al.*, Seeded growth of highly crystalline molybdenum disulphide monolayers at controlled locations, Nat. Commun. **6**, 6128 (2015).

[29] F. Schwierz, J. Pezoldt, and R. Granzner, Two-dimensional materials and their prospects in transistor electronics, Nanoscale **7**, 8261 (2015).

[30] P. Hu, J. Ye, X. He, K. Du, K. K. Zhang, X. Wang, Q. Xiong, Z. Liu, H. Jiang, and C. Kloc, Control of radiative exciton recombination by charge transfer induced surface dipoles in MoS_2 and WS_2monolayers, Sci. Rep. **6**, 24105 (2016).

[31] M. S. Kim, S. J. Yun, Y. Lee, C. Seo, G. H. Han, K. K. Kim, Y. H. Lee, and J. Kim, Biexciton emission from edges and grain boundaries of triangular WS_2 monolayers, ACS Nano **10**, 2399 (2016).

[32] J. He, N. Kumar, M. Z. Bellus, H.-Y. Chiu, D. He, Y. Wang, and H. Zhao, Electron transfer and coupling in graphene-tungsten disulfide van der Waals heterostructures, Nat. Commun. **5**, 5622 (2014).

[33] K. Kang, K. Godin, Y. D. Kim, S. Fu, W. Cha, J. Hone, and E. H. Yang, Graphene-assisted antioxidation of tungsten disulfide monolayers: Substrate and electric-field effect, Adv. Mater. **29**, 1603898 (2017).

[34] M. O'Brien, N. McEvoy, D. Hanlon, T. Hallam, J. N. Coleman, and G. S. Duesberg, Mapping of low-frequency Raman modes in CVD-grown transition metal dichalcogenides: Layer number, stacking orientation and resonant effects, Sci. Rep. **6**, 19476 (2016).

[35] W. Zhao, Z. Ghorannevis, K. K. Amara, J. R. Pang, M. Toh, X. Zhang, C. Kloc, P. H. Tan, and G. Eda, Lattice dynamics in mono- and few-layer sheets of WS_2 and WSe_2, Nanoscale **5**, 9677 (2013).

[36] Y. Kobayashi, S. Sasaki, S. Mori, H. Hibino, Z. Liu, K. Watanabe, T. Taniguchi, K. Suenaga, Y. Maniwa, and Y. Miyata, Growth and optical properties of high-quality monolayer WS_2 on graphite, ACS Nano **9**, 4056 (2015).

[37] H. R. Gutie, N. Perea-lo, A. Laura, A. Berkdemir, B. Wang, and M. Terrones, Extraordinary room-temperature photoluminescence in triangular WS_2 monolayers, Nano Lett. **13**, 3447 (2013).

[38] A. Molina-Sánchez and L. Wirtz, Phonons in single-layer and few-layer MoS_2 and WS_2, Phys. Rev. B **84**, 155413 (2011).

[39] J. E. Lee, G. Ahn, J. Shim, Y. S. Lee, and S. Ryu, Optical separation of mechanical strain from charge doping in graphene, Nat. Commun. **3**, 1024 (2012).

[40] X. Huang, Y. Gao, T. Yang, W. Ren, H.-M. Cheng, and T. Lai, Quantitative analysis of temperature dependence of Raman shift of monolayer WS_2, Sci. Rep. **6**, 32236 (2016).

[41] M. W. Iqbal, M. Z. Iqbal, M. F. Khan, M. A. Shehzad, Y. Seo, and J. Eom, Deep-ultraviolet-light-driven reversible doping of WS_2 field-effect transistors, Nanoscale **7**, 747 (2014).

[42] F. Wang, I. A. Kinloch, D. Wolverson, R. Tenne, A. Zak, E. O'Connell, U. Bangert, and R. J. Young, Strain-induced phonon shifts in tungsten disulfide nanoplatelets and nanotubes, 2D Mater. **4**, 1 (2016).

[43] A. Berkdemir, H. R. Gutiérrez, A. R. Botello-Méndez, N. Perea-López, A. L. Elías, C.-I. Chia, B. Wang, V. H. Crespi, F. López-Urías, J.-C. Charlier *et al.*, Identification of individual and few layers of WS_2 using Raman spectroscopy, Sci. Rep. **3**, 1755 (2013).

[44] F. Withers, T. H. Bointon, D. C. Hudson, M. F. Craciun, and S. Russo, Electron transport of WS_2 transistors in a hexagonal boron nitride dielectric environment, Sci. Rep. **4**, 4967 (2015).

[45] G. V. Bianco, M. Losurdo, M. M. Giangregorio, A. Sacchetti, P. Prete, N. Lovergine, P. Capezzuto, and G. Bruno, Direct epitaxial CVD synthesis of tungsten disulfide on epitaxial and CVD graphene, RSC Adv. **5**, 98700 (2015).

[46] H. Henck, D. Pierucci, J. Chaste, C. H. Naylor, J. Avila, A. Balan, M. G. Silly, M. C. Asensio, F. Sirotti, A. T. Charlie Johnson, E. Lhuillier, and A. Ouerghi, Electrolytic phototransistor based on graphene-MoS_2 van der Waals p-n heterojunction with tunable photoresponse, Appl. Phys. Lett. **109**, 113103 (2016).

[47] X. Mao, Y. Xu, Q. Xue, W. Wang, and D. Gao, Ferromagnetism in exfoliated tungsten disulfide nanosheets, Nanoscale Res. Lett. **8**, 430 (2013).

[48] Y. Li, D. Chen, and R. A. Caruso, Enhanced electrochromic performance of WO_3 nanowire networks grown directly on fluorine-doped tin oxide substrates, J. Mater. Chem. C **4**, 10500 (2016).

[49] D. Barrera, Q. Wang, Y.-J. Lee, L. Cheng, M. J. Kim, J. Kim, and J. W. P. Hsu, Solution synthesis of few-layer 2H MX2 (M = Mo,W; X = S,Se), J. Mater. Chem. C **5**, 2859 (2017).

[50] Y. Gao, Z. Liu, D.-M. Sun, L. Huang, L.-P. Ma, L.-C. Yin, T. Ma, Z. Zhang, X.-L. Ma, L.-M. Peng *et al.*, Large-area synthesis of high-quality and uniform monolayer WS_2 on reusable Au foils, Nat. Commun. **6**, 8569 (2015).

[51] S. Y. Zhou, G.-H. Gweon, A. V. Fedorov, P. N. First, W. A. De Heer, D.-H. Lee, F. Guinea, A. H. C. Neto, and A. Lanzara, Substrate-induced bandgap opening in epitaxial graphene, Nat. Mater. **6**, 770 (2007).

[52] H. Coy Diaz, R. Addou, and M. Batzill, Interface properties of CVD grown graphene transferred onto MoS_2(0001), Nanoscale **6**, 1071 (2014).

[53] H. C. Diaz, J. Avila, C. Chen, R. Addou, M. C. Asensio, and M. Batzill, Direct observation of interlayer hybridization and Dirac relativistic carriers in graphene/MoS_2 van der Waals heterostructures, Nano Lett. **15**, 1135 (2015).

[54] P. Giannozzi, S. Baroni, N. Bonini, M. Calandra, R. Car, C. Cavazzoni, D. Ceresoli, G. L. Chiarotti, M. Cococcioni, I. Dabo *et al.*, QUANTUM ESPRESSO: A modular and open-source software project for quantum simulations of materials, J. Phys.: Condens. Matter **21**, 395502 (2009).

[55] O. Andreussi, T. Brumme, O. Bunau, M. Buongiorno Nardelli, M. Calandra, R. Car, C. Cavazzoni, D. Ceresoli, M. Cococcioni, N. Colonna *et al.*, Advanced capabilities for materials modelling with Quantum ESPRESSO, J. Phys.: Condens. Matter **29**, 465901 (2017).

[56] J. P. Perdew, K. Burke, and M. Ernzerhof, Generalized Gradient Approximation Made Simple, Phys. Rev. Lett. **77**, 3865 (1996); Generalized Gradient Approximation Made Simple, **78**, 1396(E) (1997).

[57] A. V. Krukau, O. A. Vydrov, A. F. Izmaylov, and G. E. Scuseria, Influence of the exchange screening parameter on the performance of screened hybrid functionals, J. Chem. Phys. **125**, 224106 (2006).

[58] L. Lin, Adaptively compressed exchange operator, J. Chem. Theory Comput. **12**, 2242 (2016).

[59] T. Brumme, M. Calandra, and F. Mauri, First-principles theory of field-effect doping in transition-metal dichalcogenides: Structural properties, electronic structure, Hall coefficient, and electrical conductivity, Phys. Rev. B **91**, 155436 (2015).

[60] D. R. Hamann, Optimized norm-conserving Vanderbilt pseudopotentials, Phys. Rev. B **88**, 085117 (2013).

[61] P. Scherpelz, M. Govoni, I. Hamada, and G. Galli, Implementation and validation of fully relativistic GW calculations: Spin–orbit coupling in molecules, nanocrystals, and solids, J. Chem. Theory Comput. **12**, 3523 (2016).

[62] H. M. Hill, A. F. Rigosi, K. T. Rim, G. W. Flynn, and T. F. Heinz, Band alignment in MoS_2/WS_2 transition metal dichalcogenide heterostructures probed by scanning tunneling microscopy and spectroscopy, Nano Lett. **16**, 4831 (2016).

[63] A. Chernikov, T. C. Berkelbach, H. M. Hill, A. Rigosi, Y. Li, O. B. Aslan, D. R. Reichman, M. S. Hybertsen, and T. F. Heinz, Exciton Binding Energy and Nonhydrogenic Rydberg Series in Monolayer WS_2, Phys. Rev. Lett. **113**, 076802 (2014).

[64] S. Ulstrup, A. G. Čabo, D. Biswas, J. M. Riley, M. Dendzik, C. E. Sanders, M. Bianchi, C. Cacho, D. Matselyukh, R. T. Chapman *et al.*, Spin and valley control of free carriers in single-layer WS_2, Phys. Rev. B **95**, 041405(R) (2017).